Direct real-time observation of actin filament branching mediated by Arp2/3 complex using total internal reflection fluorescence microscopy

Kurt J. Amann* and Thomas D. Pollard*†‡

*The Salk Institute for Biological Studies, Structural Biology Laboratory, 10010 North Torrey Pines Road, La Jolla, CA 92037; and †Department of Molecular, Cellular, and Developmental Biology, Yale University, New Haven, CT 06520

Contributed by Thomas D. Pollard, October 18, 2001

Existing methods for studying actin filament dynamics have allowed analysis only of bulk samples or individual filaments after treatment with the drug phalloidin, which perturbs filament dynamics. Total internal reflection fluorescence microscopy with rhodamine-labeled actin allowed us to observe polymerization in real time, without phalloidin. Direct measurements of filament growth confirmed the rate constants measured by electron microscopy and established that rhodamine actin is a kinetically inactive tracer for imaging. In the presence of activated Arp2/3 complex, growing actin filaments form branches at random sites along their sides, rather than preferentially from their barbed ends.

Actin filament polymerization produces forces that push forward the leading edge of motile cells (1), as well as some subcellular structures (2), organelles (3), and intracellular pathogens (4). Additionally, once polymerized, actin filaments serve as substrates for myosin motors and provide mechanical structure for eukaryotic cells. Elucidating the mechanisms regulating actin polymerization is crucial to understanding fundamental issues of cellular structure and motility. Bulk biochemical methods for studying actin polymerization have been available for more than a half-century (5) and were initially useful for determining the conditions required for shifting the monomer-polymer equilibrium. Later electron microscopic studies allowed filament elongation rates to be determined directly by measuring their lengths after elongating for known periods (6–8). More recent studies using fluorescently labeled phalloidin to visualize filaments have allowed direct visualization of filament severing (9–11) and have shown the products of annealing (12) and branch formation mediated by Arp2/3 complex (13, 14). However, because phalloidin stabilizes filaments, it is not well suited for observing filament dynamics. Although actin can be labeled directly with fluorophores on a reactive cysteine residue near the carboxyl terminus, visualization of filament elongation by wide field fluorescence illumination has been limited by the high background fluorescence from both out-of-focus filaments and particularly the labeled actin monomers that are required to drive the reaction.

We have overcome these obstacles by using total internal reflection fluorescence microscopy (TIRFM) to visualize individual filaments of partially labeled rhodamine actin bound to *N*-ethyl maleimide (NEM) myosin on the illuminated surface of flow cells. The background fluorescence from monomers is minimized, because only a thin section of sample is illuminated (15) by virtue of an evanescent wave created at the surface of the supporting glass slide. NEM inhibits myosin motor activity but allows actin filament binding, even in ATP (16). We observed actin filament elongation and branch formation mediated by Arp2/3 complex in real time. Direct measurements of filament growth confirmed the rate constants measured by electron microscopy (6, 8) and established that rhodamine actin is a kinetically inactive tracer for imaging. In the presence of activated Arp2/3 complex, growing actin filaments formed branches at random sites along their sides, rather than preferentially from their barbed ends, providing further support for the side-binding model for dendritic nucleation (13, 17, 18).

Materials and Methods

Proteins. Actin was isolated from rabbit skeletal muscle (19) and further purified by gel filtration on Sephacryl S-300. To label actin on Cys-374 with rhodamine, 60 μM actin was polymerized and DTT was removed by dialysis for 2 h against 2 mM Tris·HCl (pH 8.0), 50 mM KCl, 1 mM $MgCl_2$, 200 μM ATP. A 5-fold molar excess of 5′-rhodamine-maleimide (Molecular Probes) was added and mixed at 4°C overnight. Labeled actin was centrifuged at 300,000 $\times$ *g* for 30 min. Unpolymerized, labeled actin in the supernatant was dialyzed into Ca-G buffer (2 mM Tris·HCl, pH 8.0/500 μM DTT/200 μM ATP/100 μM $CaCl_2$), gel-filtered on Sephacryl S-300, and after a 2-h incubation in Ca-G buffer containing 50 mM KCl again gel-filtered with the same buffer. Labeling stoichiometry was determined by using a molar extinction coefficient for rhodamine of 80,000 at 543 nm, and actin concentrations were determined by SDS/PAGE–Coomassie blue staining and densitometry and by Bradford assay, using unlabeled actin as the standard. In all cases, the final purified actin was >99% labeled. By sedimentation equilibrium analytical ultracentrifugation, purified rhodamine actin was monomeric under both polymerizing and nonpolymerizing conditions. To ensure that rhodamine actin was competent for copolymerization with unlabeled actin, before use rhodamine actin was polymerized with a 1:1 ratio of unlabeled actin for 3 h at 4°C, and centrifuged at 400,000 $\times$ *g* for 30 min. Pellets, containing ~40% rhodamine actin, were suspended in Ca-G buffer and dialyzed against the same buffer for 2 days. Actin was again centrifuged in Ca-G buffer before use. Rabbit skeletal muscle myosin was inactivated by incubation with 1 mM NEM for 40 min at 22°C, and the reaction was quenched with 25 mM DTT. NEM myosin was stored in 50% glycerol and diluted to 100 μg/ml in Mg-G buffer containing 500 mM KCl before use. Arp2/3 complex from bovine thymus (20), *Acanthamoeba* profilin-I (21), and recombinant human Scar-I WA (18, 22) were prepared by D. Kaiser, The Salk Institute.

Microscopy. An Olympus IX-70 inverted microscope (18) was modified for TIRF illumination. A 100-mW Kr/Ar laser (Melles Griot, Carlsbad, CA) emitting 40 mW in each of 488- and 568-nm

Abbreviations: NEM, *N*-ethyl maleimide; TIRFM, total internal fluorescence microscopy.

‡To whom reprint requests should be addressed. E-mail: thomas.pollard@yale.edu.

The publication costs of this article were defrayed in part by page charge payment. This article must therefore be hereby marked "*advertisement*" in accordance with 18 U.S.C. §1734 solely to indicate this fact.

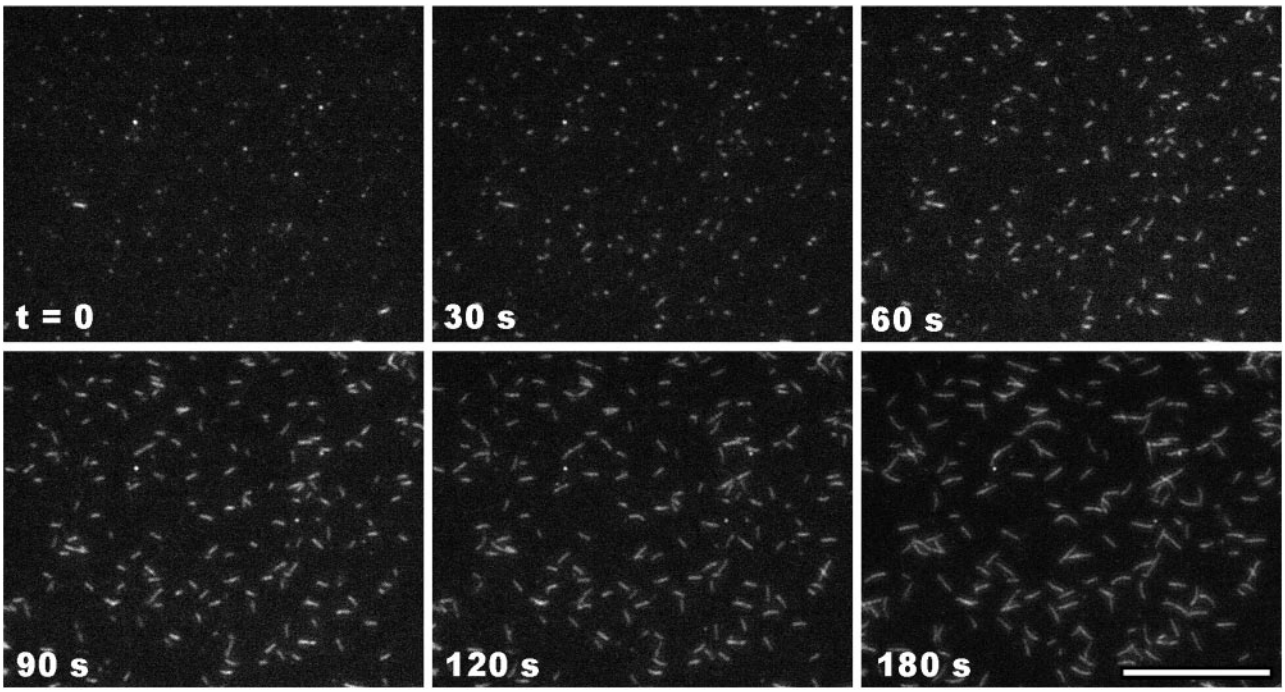

Fig. 1. Elongation of actin filaments visualized by TIRFM. Actin monomers (1 μM, 40% rhodamine-labeled) were polymerized in fluorescence buffer (50 mM KCl/1 mM $MgCl_2$/10 mM imidazole, pH 7.0/1 mM EGTA/100 μM $CaCl_2$/200 μM ATP/3 mM NaN_3/3 mg/ml glucose/100 μg/ml glucose oxidase/20 μg/ml catalase/10 mM DTT) in a flow cell with the coverslip coated with 100 μg/ml NEM-myosin for 1 min, and blocked with 1% BSA for 1 min. Exposures of 300 ms were collected every 3 s for 3 min. Shown are frames representing the time course of elongation. (Scale bar = 14 μm.)

emission lines through a 3× beam expander (Melles Griot no. 09 LBZ 001) was used as the light source. D488/10X and D568/10X bandpass filters (Chroma Technology, Brattleboro, VT) were used as excitation filters. A 100-mM focal length plano-convex lens focused the beam through a 40 × 23.5 mm Pellin-Broca prism (CVI Laser, Livermore, CA) on a layer of glycerol on flow cells above a 1.35 numerical aperture, ×100 objective lens. Flow cells were constructed by mounting a 24 × 60-mm no. 0 coverslip perpendicularly across a standard 25 × 75 × 1-mm microscope slide, separated by two 5-mm-wide strips of Parafilm, stretched tightly and placed 5 mm apart. The resulting chambers measured ~30 μm in height and held a volume of 5 μl. Filament polymerization was observed by adding partially labeled monomeric actin to polymerization buffer and immediately flowing the solution into the cell. The microscope could be focused and images were captured typically within 30 s after inducing polymerization.

Image and Data Analysis. Exposures of rhodamine-actin samples (100–300 ms) were collected by using a Hamamatsu C4742-95 cooled charge-coupled device camera. Images were processed and movies were produced by using METAMORPH 4.5 (Universal Imaging, Media, PA). Filament lengths could be accurately measured to ~250 nm (13). Elongation rates were determined by measuring filament lengths from at least six frames separated by at least 15 s each. Linear fits were made to the plots of length versus time, with the slope representing the elongation rate. Elongation rates were converted from $\mu m \cdot s^{-1}$ to s^{-1} by dividing by 370 actin monomers per micrometer. Correlation coefficients for single filament elongation plots exceeded 0.95, confirming that elongation rates were constant. Because calculation of elongation rates depended on accurate measurement of length changes, rather than absolute lengths, the fluorescence halo effect did not affect the results. As a result, length changes of as little as 100 nm could be measured. Movies were prepared in METAMORPH, using Cinepak Codec compression, and are shown at ×30 time compression.

Results and Discussion

TIRFM revealed individual filaments in flow cells containing 1 μM actin filaments labeled with equimolar rhodamine-phalloidin, whereas no filaments were discernable by epifluorescence because of the high background fluorescence. Similar results were found when filaments of 40% rhodamine actin stabilized with unlabeled phalloidin were examined by epifluorescence and TIRFM. When 1 μM polymerized 40% rhodamine actin was examined by TIRFM without phalloidin, individual, surface-bound filaments were observed. Although some background fluorescence was present with TIRFM, it was significantly less than the epifluorescence background (data not shown).

TIRFM allowed direct, real-time imaging of elongating actin filaments (Fig. 1). The robustness of the assay is best appreciated by viewing movies of filament elongation (Movie 1, which is published as supporting information on the PNAS web site, www.pnas.org). The elongation rate depended on both the concentration of actin and the fraction of rhodamine-labeled actin. At actin concentrations lower than 0.3 μM, elongation was too slow to measure accurately, whereas at concentrations greater than 2 μM, the high spontaneous nucleation rate produced filaments too numerous to resolve. Between 0.3 and 2 μM, however, the number of filaments per field varied roughly in proportion to the concentration. Significant growth was observed only at only one end, the barbed end (Fig. 1). Filament barbed ends grew steadily at constant rates for at least 5 min, indicating that the monomer pool was not appreciably depleted by polymerization. The barbed-end elongation rate was directly proportional to the actin concentration over the range tested, yielding an elongation rate constant of 5.5 $\mu M^{-1} \cdot s^{-1}$ for 40% labeled actin (Fig. 2*A*). Extrapolation of the elongation rate to

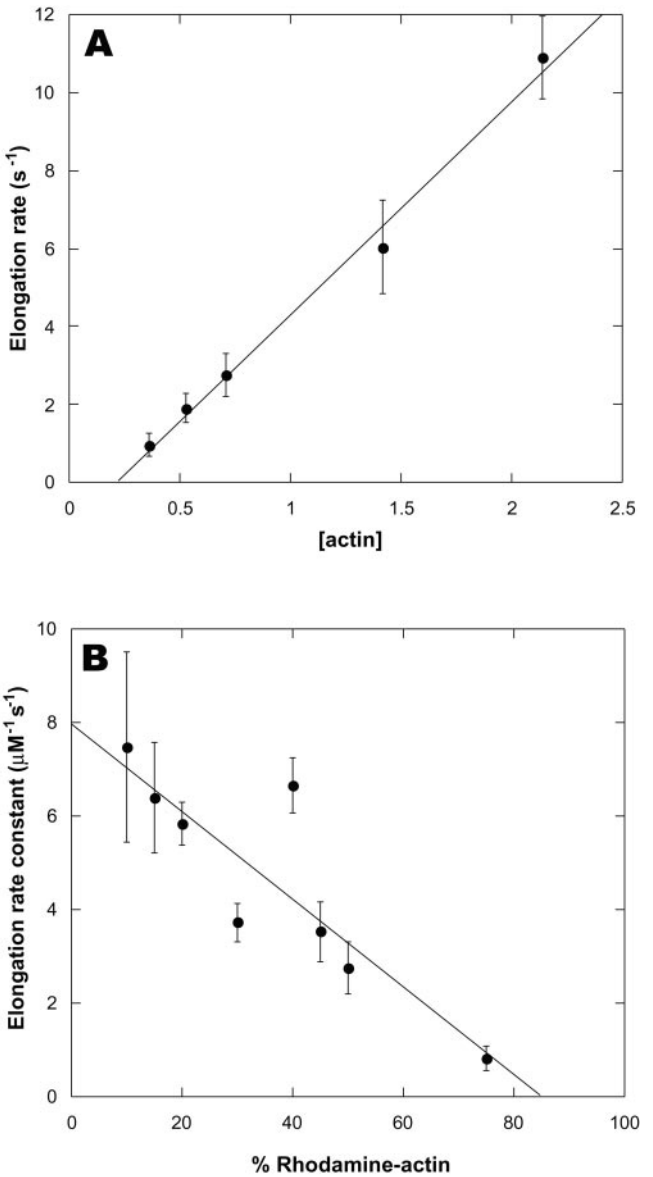

Fig. 2. Dependence of barbed-end elongation rates on actin monomer concentration. Actin filament elongation was observed as described in Fig. 1. (*A*) Dependence on total actin concentration with constant 40% rhodamine-actin. (*B*) Dependence on fraction of rhodamine-labeled actin with 1 μM total actin. Values shown are the mean ± SD of at least six randomly chosen growing filaments per condition. Lines represent linear least-squares fits to the mean values.

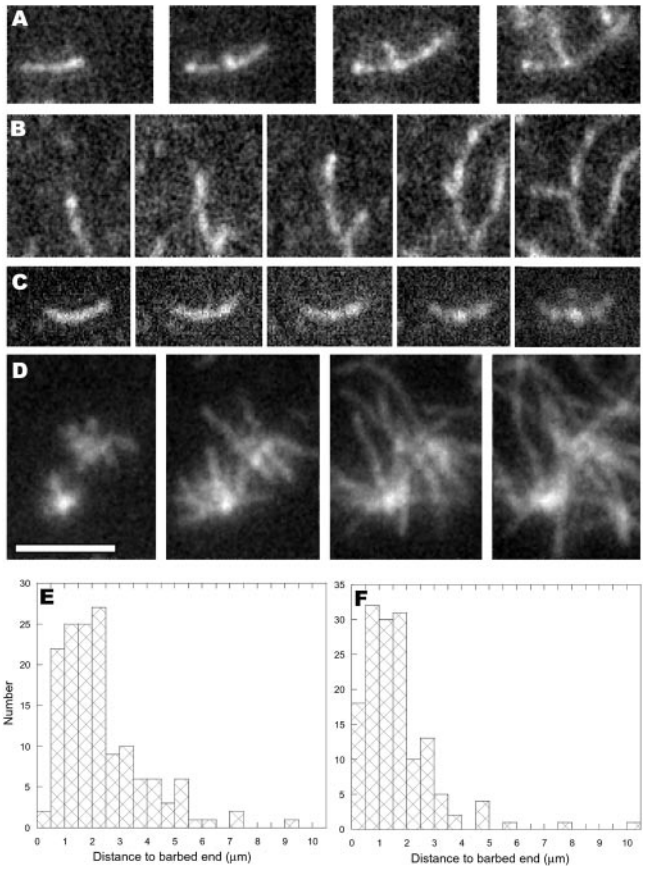

Fig. 3. Actin filament branch formation. Filament elongation of 20% rhodamine actin was visualized by TIRFM as described in Fig. 1. (*A* and *B*) Actin monomers (1 μM) were visualized polymerizing for 2 min before addition of 100 nM Arp2/3 complex, 300 nM Scar WA, and 2 μM actin monomers. Frames shown were subsequently captured at 100, 130, 170, and 210 (*A*) or 105, 135, 165, 270, and 305 (*B*) s after addition. (*C*) Actin monomers (2 μM) were polymerized for 3 min before growing branches for 3 min in the presence of 60 nM Arp2/3 complex, 500 nM Scar WA, 4 μM profilin, and 2 μM actin. Frames shown were collected at 0, 36, 75, 132, and 180 s after addition of branching mixture. (*D*) Unbound components were washed from the branched structures in *C* and 2 μM monomeric actin was added to the cell. Frames shown were collected 0, 32, 72, and 108 s after monomer addition. (*E* and *F*) Histograms of the distances from branch points to mother filament barbed ends for branches growing from the sides of filaments that had grown before addition of Arp2/3 complex (*E*) or from portions of filaments that had grown in the presence of Arp2/3 complex (*F*). (Scale bar = 4 μm.)

zero actin concentration yielded a k_- of 1.2 s^{-1}, in close agreement with electron microscopic studies (8). Occasionally during the course of observation, fully formed filaments appeared spontaneously, having elongated in solution and diffused into the plane of excitation. Because the filaments appeared so suddenly, such events were easily distinguished from filament elongation.

At a total actin concentration of 1 μM, the elongation rate was inversely proportional to the fraction of labeled actin (Fig. 2*B*). The barbed end elongation rate constant, extrapolated to 100% unlabeled actin, was 8 $\mu M^{-1} \cdot s^{-1}$, similar to values determined by electron microscopy (6, 8). The elongation rate constant extrapolated to zero at 0.22 μM total actin, which corresponded to 0.13 μM unlabeled actin (Fig. 2*A*). Similarly, the dependence of the elongation rate constant on the fraction of rhodamine actin extrapolated to zero growth at 85% rhodamine actin, which corresponded to 0.15 μM unlabeled actin. These values agree closely with the established value of 0.1 μM for the critical concentration at the barbed end. Thus, the elongation rate was determined solely by the concentration of unlabeled actin. Rhodamine actin behaved as a kinetically inactive tracer for imaging, likely because of inefficient incorporation into filaments under nonequilibrium conditions. Based on these observations we chose 20% labeled actin for subsequent experiments.

TIRFM allowed us to visualize actin filament branch formation mediated by activated Arp2/3 complex in real time (Fig. 3; Movie 2, which is published as supporting information on the PNAS web site). Filaments bound to NEM-myosin on the surface of the TIR flow cell were elongated for 3 min, before adding Arp2/3 complex, the activator Scar-WA, and additional actin monomers. These mother filaments continued to elongate at the rates determined by the monomer concentration. The

earliest indications of branch formation were bright spots appearing along the lengths of mother filaments (Fig. 3 *A–C*). The bright spots grew to become bumps protruding from the sides of filaments. After typically less than 1 min, they became recognizable as branches emanating from the sides of mother filaments (Fig. 3 *A* and *B*). The branches exhibited the 70° angle characteristic of Arp2/3 complex-mediated branches, and elongated at the same rate as mother filament barbed ends. This is further confirmation that the pointed end of the daughter filament is located at the base of the branch.

Branches arose both from the sides of filaments that had grown before addition of Arp2/3 complex and from portions of filaments that had grown in the presence of Arp2/3 complex. Although the latter observation could in principle be explained by Arp2/3 complex incorporating into the growing mother filament, the former is only reasonably explained by Arp2/3 complex binding to the side of the mother filaments. Branch density (number of branches per μm mother filament) varied with the Arp2/3 concentration, but only a relatively narrow range of concentrations (25–100 nM) produced images suitable for quantitative analysis.

Using 100 nM Arp2/3 complex, branches ($n = 146$) arose from pre-existing mother filaments (161 mother filaments, 3.56 $\pm$ 1.71 SD μm in length) at a density of one branch per 4.4 μm. The sites of branching from mother filaments were essentially random, as they occurred 2.34 $\pm$ 1.5 SD μm from the position of the barbed end at the time of Arp2/3 complex addition (Fig. 3*E*). Because short branches within 0.5 μm of mother filament barbed ends were most affected by small errors in length measurement, these branches may be slightly underrepresented in the data. Because ATP hydrolysis in actin filaments occurs at a rate of 0.3 s^{-1} (23) and P_i is released at a rate of 0.002 s^{-1} (24), the oldest portions of average mother filaments contained ~85% ADP-P_i-actin and 15% ADP actin. Because of the ~30-s delay between washing out actin monomers and addition of the branching solution, there was essentially no ATP-actin cap on the barbed ends at the time Arp2/3 complex was added. Thus, although we observed no preference for branch formation near barbed ends, the shallow gradient of ADP-P_i to ADP along the length of mother filaments would not necessarily reveal a subtle preference for branches forming on the sides of ATP- or ADP-P_i actin subunits relative to ADP subunits.

Branches also grew from portions of filaments that grew after the addition of Arp2/3 complex. From frames captured shortly after branches became visible, we measured the distance from the branch point to the barbed end of the daughter filament and both ends of the mother filament ($n = 154$). Because all barbed ends elongated at the same rate, it was possible by extrapolation back in time to determine the position of each branch on the mother filament relative to the barbed and pointed ends of the mother filament at the time that the branch started to grow. Branches arose on average 1.56 $\pm$ 1.42 SD μm from the barbed ends of mother filaments that averaged 4.0 $\pm$ 2.1 SD μm in length (Fig. 3*F*). On average, branches arose on mother filaments 40 $\pm$ 19% of the length from the barbed end of the mother filament. Of 152 branches, 116 arose from the barbed end half of the mother filament. Thirty six others arose from the pointed end half of the mother filament, some as much as 10 μm from the barbed end. Two remaining daughter filaments measured longer than their mothers. Because only ~100 nm (37 subunits) of the newest growth were composed of primarily ATP actin, with the proportion declining exponentially toward the pointed end, a preference for branch formation from ATP filaments relative to ADP-P_i or ADP filaments could underlie the modest preference for branching near the barbed ends of elongating filaments.

Because branches arose, on average, 1.56 μm from the mother filament barbed end, this means that, on average, the barbed end of the mother filament elongated past the branch point for 4 min before the branch started to grow. If Arp2/3 complex incorporated into the mother filament during its elongation as postulated (25), an average 4-min delay before branch formation would be required to explain this observation. Experiments monitoring actin polymerization by pyrene fluorescence (18, 22, 26) demonstrated unambiguously that nucleation by Arp2/3 complex proceeds within seconds in the presence of stimulatory actin filaments rather than after a substantial lag. Furthermore, epifluorescence images of filaments grown for less than 4 min in the presence of activated Arp2/3 complex show well-established branches (14, 18).

We previously demonstrated that profilin can favor Arp2/3 complex branching by reducing the spontaneous nucleation rate and nucleation from capping protein (13). Using TIRFM, we observed that profilin greatly increases the density of Arp2/3 complex branching from mother filaments (Fig. 3 *C* and *D*). When 60-nM activated Arp2/3 complex was added to mother filaments along with actin monomers and an excess of profilin, numerous branches appeared as bumps on filament sides (Fig. 3*C*; Movie 3, which is published as supporting information on the PNAS web site). The high efficiency of nucleation rapidly depleted the monomer pool, resulting in an early arrest of branch elongation. After washing out unbound components and adding additional actin monomers, the branches resumed rapid elongation (Movie 4, which is published as supporting information on the PNAS web site). The resultant branched structures (Fig. 3*D*) were composed of filaments too numerous to count accurately, resembling the "dandelion" structures observed by wide-field fluorescence microscopy at high concentrations of Arp2/3 complex (13).

TIRFM is a robust tool for analysis of actin dynamics and the proteins that control them. The ability to observe the assembly and disassembly of individual filaments in real time will serve as a valuable complement to existing analytical methodologies. In the present case, we addressed the mechanism of actin filament branching by activated Arp2/3 complex. Biochemical, microscopic, and structural analysis (13, 17, 18, 27, 28) had indicated that branch formation occurred on the sides of filaments. Nonetheless, without direct observation of the events, alternative hypotheses (14, 25) were still formally possible. Our observations show that branches form on the sides of filaments. TIRFM will similarly allow further insight into and clarification of the mechanisms of action of a wide variety of actin-associated proteins.

We thank Enrique De La Cruz or his critical evaluation of this manuscript and helpful suggestions. This work was supported by National Institutes of Health Research Grant GM26338 (to T.D.P.) and Postdoctoral Fellowship GM20638 (to K.J.A.).

1. Theriot, J. A. & Mitchison, T. J. (1991) *Nature (London)* **352,** 126–131.
2. Schafer, D. A., Welch, M. D., Machesky, L. M., Bridgman, P. C., Meyer, S. M. & Cooper, J. A. (1998) *J. Cell Biol.* **143,** 1919–1930.
3. Boldogh, I. R., Yang, H.-C., Nowakowski, W. D., Karmon, S. L., Hays, L. G., Yates, J. R., III & Pon, L. A. (2001) *Proc. Natl. Acad. Sci. USA* **98,** 3162–3167.
4. Dabiri, G. A., Sanger, J. M., Portnoy, D. A. & Southwick, F. S. (1990) *Proc. Natl. Acad. Sci. USA* **87,** 6068–6072.
5. Straub, F. B. & Feuer, G. (1949) *Biochem. Biophys. Acta* **4,** 455–470.
6. Bonder, E. M., Fishkind, D. J. & Mooseker, M. S. (1983) *Cell* **34,** 491–501.
7. Pollard, T. D. & Mooseker, M. S. (1981) *J. Cell Biol.* **88,** 654–659.
8. Pollard, T. D. (1986) *J. Cell Biol.* **103,** 2747–2754.
9. Maciver, S. K., Zot, H. G. & Pollard, T. D. (1991) *J. Cell Biol.* **115,** 1611–1620.
10. Bearer, E. L. (1991) *J. Cell Biol.* **115,** 1629–1638.
11. Ichetovkin, I., Han, J., Pang, K. M., Knecht, D. A. & Condeelis, J. S. (2000) *Cell Motil. Cytoskeleton* **45,** 293–306.

12. Andrianantoandro, E., Blanchoin, L., Sept, D., McCammon, J. A. & Pollard, T. D. (2001) *J. Mol. Biol.* **312,** 721–730.
13. Blanchoin, L., Amann, K. J., Higgs, H. N., Marchand, J. B., Kaiser, D. A. & Pollard, T. D. (2000) *Nature (London)* **404,** 1007–1011.
14. Boujemaa-Paterski, R., Goudin, E., Hansen, G., Samarin, S., Le Clainche, C., Didry, D., Dehoux, P., Cossart, P., Kocks, C., Carlier, M.-F. & Pantaloni, D. (2001) *Biochemistry* **40,** 11390–11404.
15. Axelrod, D. (1990) in *Noninvasive Techniques in Cell Biology,* eds. Foskett, J. K. & Grinstein, S. (Wiley, New York), pp. 93–127.
16. Pemrick, S. & Weber, A. (1976) *Biochemistry* **15,** 5193–5198.
17. Mullins, R. D., Heuser, J. A. & Pollard, T. D. (1998) *Proc. Natl. Acad. Sci. USA* **95,** 6181–6186.
18. Amann, K. J. & Pollard, T. D. (2001) *Nat. Cell Biol.* **3,** 306–310.
19. Spudich, J. A. & Watt, S. (1971) *J. Biol. Chem.* **246,** 4866–4871.
20. Higgs, H. N. & Pollard, T. D. (2000) *J. Cell Biol.* **150,** 1311–1320.
21. Kaiser, D. A., Sato, M., Ebert, R. & Pollard, T. D. (1986) *J. Cell Biol.* **102,** 221–226.
22. Machesky, L. M., Mullins, D. M., Higgs, H. N., Kaiser, D. A., Blanchoin, L.,May, R. C., Hall, M. E. & Pollard, T. D. (1999) *Proc. Natl. Acad. Sci. USA* **96,** 3739–3744.
23. Blanchoin, L. & Pollard, T. D. (2001) *Biochemistry*, in press.
24. Pollard, T. D., Blanchoin, L. & Mullins, R. D. (2000) *Annu. Rev. Biophys.* **29,** 545–576.
25. Pantaloni, D., Boujemaa, R., Didry, D., Gounon, P. & Carlier, M.-F. (2000) *Nat. Cell Biol.* **2,** 385–391.
26. Higgs, H. N., Blanchoin, L. & Pollard, T. D. (1999) *Biochemistry* **38,** 15212–15222.
27. Volkmann, N., Amann, K. J., Stoilova-McPhie, S., Egile, C., Winter, D. C., Hazelwood, L., Heuser, J. E., Li, R., Pollard, T. D. & Hanein, D. (2001) *Science* **293,** 2456–2459.
28. Robinson, R., Turbedsky, K., Kaiser, D. A., Higgs, H. N., Marchand, J.-B., Choe, S. & Pollard, T. D. (2001) *Science*, in press.